PSI-PR-95-22
August 1995

NEW PRECISION MEASUREMENTS OF dμd FUSION IN D_2 GAS

C. Petitjean[1], P. Ackerbauer[2], D.V. Balin[3], W.H. Breunlich[2], T. Case[4], K.M Crowe[4], H. Daniel[5], T. von Egidy[5], B. Gartner[2], F.J. Hartmann[5], P. Kammel[2,4], G. Kminek[2], B. Lauss[2], E.M. Maev[3], V.E. Markushin[1,6], J. Marton[2], M. Mühlbauer[5], G.E. Petrov[3], W. Prymas[2], W. Schott[5], G.G. Semenchuk[3], Yu.V. Smirenin[3], A.A. Vorobyov[3], N.I. Voropaev[3], J. Zmeskal[2].

[1] Paul Scherrer Institut, CH-5232 Villigen PSI, Switzerland
[2] Austrian Academy of Sciences (IMEP), A-1090 Vienna, Austria
[3] Petersburg Nuclear Physics Institute (PNPI), Gatchina 188350, Russia
[4] University of California and LBL, Berkeley/CA 94720, USA
[5] Technical University of Munich (TUM), D-85747 Garching, Germany
[6] Russian Research Center, Kurchatov Institute, Moscow 123182, Russia

Invited Paper presented to the International Symposium on MUON CATALYZED FUSION
μCF-95, Physics of Exotic Atoms and Molecules
Dubna, June 19-24, 1995

Paul Scherrer Institut
Würenlingen and Villigen
CH-5232 Villigen / PSI

Telephone 056 99 21 11
Telefax 056 99 21 99
Telex 82 74 14 psi ch

PSI-PR-95-22

New Precision Measurements of $d\mu d$ Fusion in D_2 Gas

C. PETITJEAN[1], P. ACKERBAUER[2], D.V. BALIN[3], W.H. BREUNLICH[2], T. CASE[4], K.M. CROWE[4], H. DANIEL[5], T. VON EGIDY[5], B. GARTNER[2], F.J. HARTMANN[5], P. KAMMEL[2,4], G. KMINEK[2], B. LAUSS[2], E.M. MAEV[3], V.E. MARKUSHIN[1,6], J. MARTON[2], M. MÜHLBAUER[5], G.E. PETROV[3], W. PRYMAS[2], W. SCHOTT[5], G.G. SEMENCHUK[3], YU.V. SMIRENIN[3], A.A. VOROBYOV[3], N.I. VOROPAEV[3], J. ZMESKAL[2]

[1] *Paul Scherrer Institut, CH-5232 Villigen PSI, Switzerland*
[2] *Austrian Academy of Sciences (IMEP), A-1090 Vienna, Austria*
[3] *Petersburg Nuclear Physics Institute (PNPI), Gatchina 188350, Russia*
[4] *University of California and LBL, Berkeley/CA 94720, USA*
[5] *Technical University of Munich (TUM), D-85747 Garching, Germany*
[6] *Russian Research Center, Kurchatov Institute, Moscow 123182, Russia*

Abstract

Reviewing $d\mu d$ fusion the motivation for a precision experiment is discussed. A new Gatchina ionization chamber surrounded by 12 neutron counters was used to observe dd-fusion in D_2-gas of 4.9% density at temperatures between 50 K and 300 K. The first results include absolute rates for $d\mu d$ formation and μd spin flip with 0.5%-2% precision and new information about the $(^3\mathrm{He} + n)/(p + t)$ ratio.

1 Introduction

The fusion of deuterium nuclei by the process chain

$$\mu d + d \rightarrow d\mu d \begin{array}{ll} \nearrow & \mu + {}^3\mathrm{He} + n \quad (1) \\ \rightarrow & \mu^3\mathrm{He} + n \quad (2) \\ \searrow & \mu + p + t \quad (3) \end{array}$$

is the longstanding reference case of Muon Catalyzed Fusion(μCF). 30 years ago (1964-66) Dzhelepov et al. [1] discovered in Dubna the *temperature dependence of $d\mu d$ formation.* Soon thereafter Vesman [2] suggested the *resonance mechanism* that correctly explained the observed temperature effects. It followed then at Dubna a decade of significant progress and interplay between theory [3, 4] and experiment [5] that led to the famous temperature resonance curve $\lambda_{d\mu d}(\mathrm{T})$ of $d\mu d$ formation in deuterium (Fig. 1). The general picture about $d\mu d$ fusion was extended during the eighties by the discovery and demonstration of hyperfine effects at PSI [6, 7] and by the inclusion of the hyperfine structure (hfs) in the theory [8, 9]. The main features of kinetics are today well established and were confirmed by a large number of measurements at the laboratories PNPI/Gatchina [10-12],PSI/Villigen [13-15],LAMPF/Los Alamos [16] and JINR/Dubna [17, 18]. Detailed discussions of the present situation in theory were recently published in [19, 20]. Fig. 1 illustrates all published data on "steady state" $d\mu d$ formation and the theory [20].

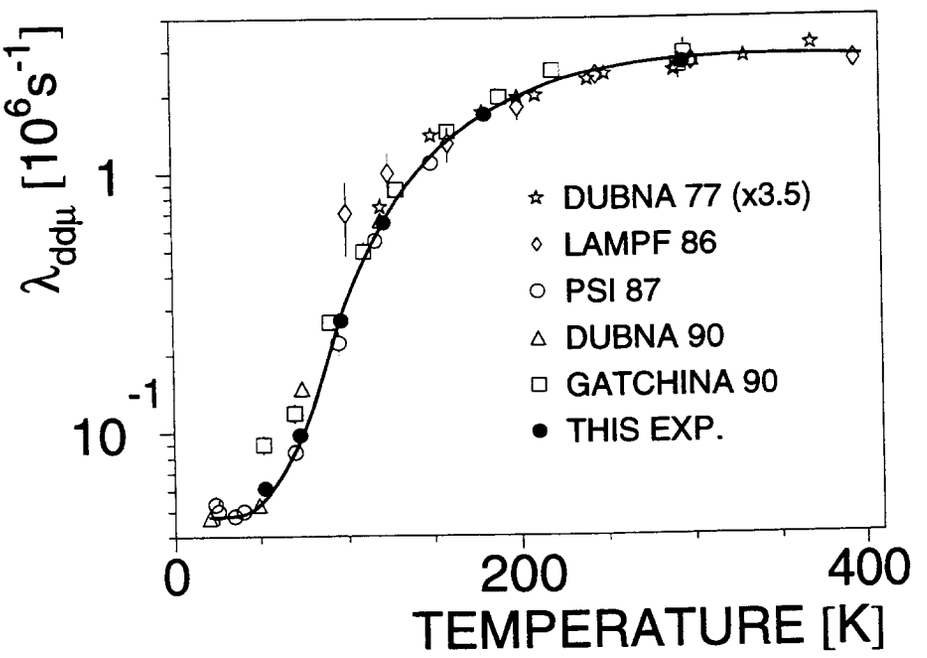

Figure 1: Temperature dependence of steady state $d\mu d$ formation rate $\lambda_{d\mu d}$.

2 Motivation

Our motivation for new measurements of $d\mu d$ fusion is founded by two aspects: The very well understood physics of this μCF cycle allowing detailed studies of specific problems *and* our capability to perform with the high muon luminosities available at PSI more precise and complete experiments than in the past. Very similar programs have been recently realized at PSI in related topics, i.e. experiments on the direct observation of dt-sticking [21, 22, 23] and a new precision measurement of the μ^3He nuclear capture rate [24, 25]. In all of these experiments the advantage of counter techniques with fast timing and event-mode data collection was combined with the excellent properties of the Gatchina high pressure ionization chamber (IC) [11, 26, 27] as a 100% efficient detector of charged particles. This setup allows the simultaneous measurement of multiple reaction channels and of the charged as well as the neutral reaction products. The physics issues addressed by our experiment are summarized as follows:

1 The measurement of absolute $d\mu d$ formation rates λ_F from μd hfs states F=1/2, 3/2. The existing neutron data are limited in absolute precision to about 5 - 10% accuracy, that is not sufficient for a full comparison with theory [20]. At temperatures below 100 K there are significant discrepancies among different data sets.

2 The branching ratio R_n/R_p between the output channels $(n + {}^3\mathrm{He})$ and $(p+t)$ which depends on the initial state J of the $d\mu d$ molecule [28] because the branching ratios for the dd fusion near threshold for the S-wave and P-wave differ by a factor of about 1.5 (see [29]). The ratio R_n/R_p is thus directly sensitive to any contribution of non resonant $d\mu d_{J=0}$ formation followed by S-wave fusion, since resonant formation leads entirely to the $d\mu d_{J=1}$ state with P-wave fusion. The first measurement of R_n/R_p was done at Gatchina [12]. Although an effect was found in agreement with the theory, more precise measurements are needed in order to separate resonant from non-resonant components of $d\mu d$ formation.

3 Investigations of sticking and stripping. The sticking probability for the channel $d\mu d \rightarrow \mu^3\mathrm{He} + n$ was determined as $\omega_d = (12.2 \pm 0.2)\%$ [10, 11] in very good agreement with theory [30, 31]. A check of this result is important, since it bears upon other measurements of dt-sticking [32] which seem to differ from theory. The probability of muon stripping during the μ^3He slowdown is predicted to be $\sim 11\%$ [33, 34]. Its verification will test the theory of stripping. We expect an important impact on the understanding of dt-sticking.

4 The μd spin-flip rate $\lambda_{3/2,1/2}$ in deuterium. There is a large unexplained discrepancy of $\sim 30\%$ [19, 20] between the theoretical predictions and all experimental observations. A precision measurement over a wide temperature range will help to identify the incorrect term in the theoretical description.

3 The Experiment

Figure 2 shows (a) the general layout of our apparatus and (b) the geometrical details of the IC detector in the center. More detailed descriptions of our experimental setup, which was already used in several previous experiments, can be found in literature [21-26]. Muons are stopped in the IC which works simultaneously as active muon target and as detector for the charged particles from *dd*-fusions. The IC is mounted with a cooling jacket inside a high vacuum vessel to allow temperature variations from 30 K to 350 K. It was filled with highly purified D_2 gas of 43.5 bar (at 300 K) corresponding to the density $\phi = 0.049 \pm 0.001$. [1] Around the vacuum chamber five thin plastic detectors identified charged particles (electrons), and ten thick plastic and two NE213 liquid neutron detectors measured the neutrons from *dd*-fusion.

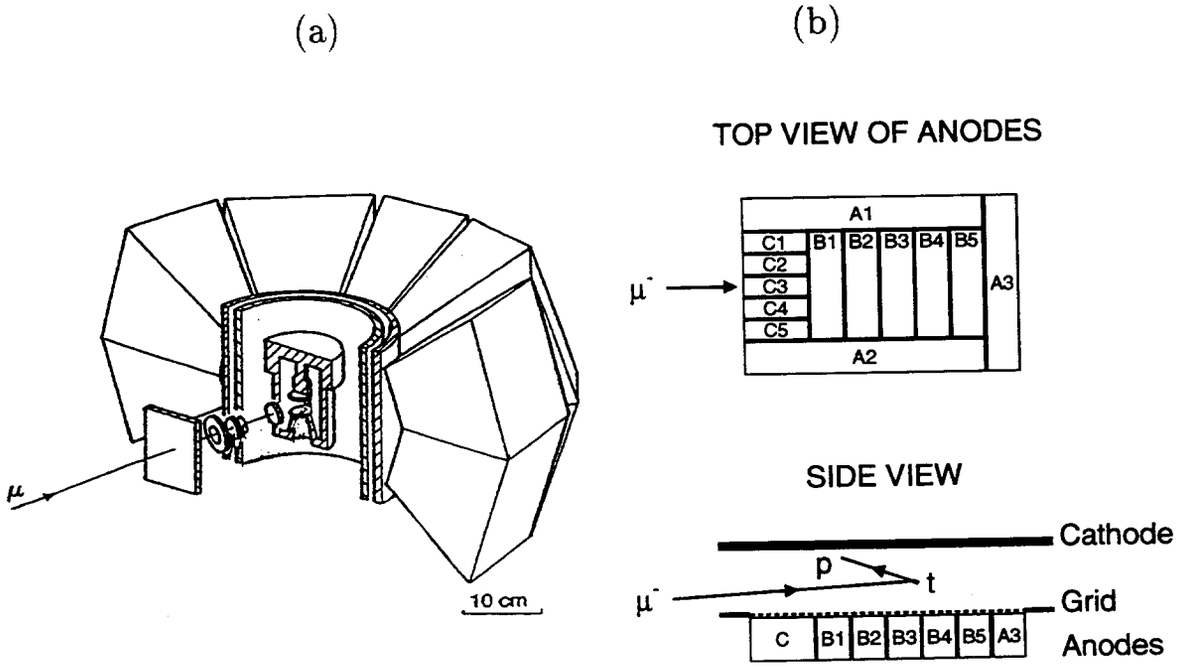

Figure 2: Experimental setup: (a) Cut away stereo view of the whole detector arrangement, (b) Geometry of the ionization chamber (IC) located in the center.

The present IC is a development from earlier Gatchina models [10-12,27] and uses a modified geometry (the same as in experiment [24, 25]) with 1.5 cm gap size and 26 cm^2 anode area. The electric field in the gap between the cathode and the gridded anode is ~24 kV/cm. The drift velocity for electrons depends on the gas density and is at our conditions 10 $mm/\mu s$. By applying offline cuts on the drift time of muon signals, the vertical acceptance of muon stops is confined and kept away from top

[1] $\phi = 1$ is the density of liquid hydrogen, $4.25 \cdot 10^{22}$ atoms/cm^3

and bottom walls. The anode is divided into 13 electrically insulated areas, of which five constitute the central detector area of 10 cm^2, while the other anodes view the charges of entering muons or escaping particles. Restricting μ-stops to the center anodes, thus defines an exact fiducial volume for the precise absolute determination of reaction rates. Each anode has independent electronics and amplifier circuits. If a signal above a low threshold ("E_{low}" $\sim$ 120 keV) is sensed, the charge of this anode is digitized by 8-bit flash ADC's for a period of 10 μs and recorded by the computer. The event triggers are generated from the summed up signal of the center anodes according to the following criteria:

(a) E_{low}-trigger: One low energy signal during the first 1.5 μs (μ drift time) signaling an incoming muon.

(b) $E_{low,low}$-trigger: Two separate signals ($\Delta t \geq 0.3\mu s$) within 10 μs indicating a muon stop followed by a fusion event separated in time.

(c) E_{high}-trigger: A signal above a high energy threshold ($\sim$800 keV) indicating a $(p+t)$ fusion event or a ^{3}He signal piling up with the muon charge.

Since the rate of muon stops was much larger than the fusion triggers and could not be processed in globo, the E_{low}-trigger was prescaled by 100. This procedure gave $\sim$5 Hz of E_{low}-triggers, while the fusion events were collected at $\sim$20 Hz. The overall efficiency for detecting charged fusion products inside the fiducial IC volume was 100%, the efficiency for detecting *dd*-neutrons by the counter array $\sim$18%. During four weeks of data taking it was operated at eight different temperatures between 50 K and 300 K. At typical run conditions the muon rates were 3000/s identified by a beam telescope of 2 cm^2 acceptance, 1000/s seen by the IC as gas stops and 300/s accepted as "good stops" in the fiducial volume ($\sim$7 cm^3) defined for absolute rate calibrations.

Fig. 3 shows two energy spectra, one measured at low temperature (53 K), the other one taken at room temperature (295 K). These spectra contain all single fusion IC events which are separated in time from the μ-stop signal. At low temperature, the peaks can be clearly attributed as follows (the identified energy ranges and the original particle energies E_o are also given):

- (0.35-0.64 MeV) ^{3}He events, E_o = 0.82 MeV, see Eq.(1)
- (0.64-0.83 MeV) μ^3He events, E_o = 0.80 MeV, see Eq.(2)
- (0.83-1.28 MeV) (^{3}He+^{3}He) pileup events (double fusions), E_{tot}= 1.6 MeV
- (1.28-3.3 MeV) $(p+t)$ events, see Eq.(3), with proton charges escaping in vertical directions (the track length of protons is 17 mm, that of tritons only 1.2 mm), $E < 4.0$ MeV ($\sim 2\%(p+t)$-^{3}He pileup events are also contained)
- (3.3-4.2 MeV) $(p+t)$ events confined to the inner volume, E_o = 4.0 MeV

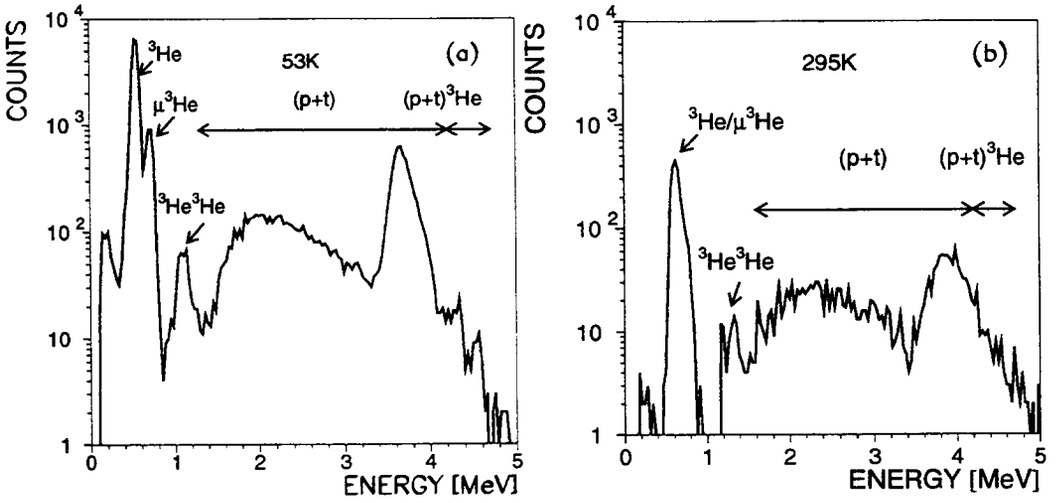

Figure 3: Energy spectra of anode signals from $d\mu d$ fusion (single fusion events) measured (a) at $T = 53$ K, (b) at $T = 295$ K.

- (4.2-4.7 MeV) $(p + t)$ +^{3}He pileup events (double fusions), E_{tot}= 4.8 MeV

Evidently, the identified energy ranges are smaller than the original energies, which is the result of *charge recombination.* The energy separation between ^{3}He and μ^3He events is caused by the stronger recombination for the heavier ionizing $^3He^{++}$ tracks than that for the single charged μ^3He^+ tracks. This recombination effect allows the direct determination of the *dd* sticking probability with high accuracy [10, 11]. At higher temperature (T $\geq$ 100 K) the recombination effect diminishes at the density chosen for our experiment, see Fig. 3b, making the evaluation of sticking impractical.

For each temperature setting independent time distributions of single fusion events (^{3}He or μ^3He) and $(p + t)$ with absolute normalization were generated, see Figs. 8 - 13 (a,b) in the appendix. Due to the effects of muon pileup, these spectra are cut off near time zero. (The $p + t$ spectra are cut more severely, because the signals have widths up to 2.2 μs, while the widths of ^{3}He/μ^3He events are below 0.5 μs.)

With the help of the neutron counter array, time spectra n + (^{3}He/μ^3He) over the full analysis range 0 - 7 μs were generated, see Figs. 8 - 13 (c) in the appendix. The spectra are a superposition of two types of IC events, both measured in coincidence with the neutron signals: (i) μ-^{3}He pileup events ($\Delta t_{\mu-^3He} \leq 0.5\ \mu s$), (ii) time separated μ + ^{3}He events ($0.3 \leq \Delta t \leq 7\ \mu s$). Combining (i) and (ii), yields undistorted time spectra from 0 to 7 μs with sharp timing and very low background, though at reduced statistics and without absolute normalization.

Finally, $(p+t)$ time spectra with selection of small drift time widths ($\Delta t \leq 0.6\ \mu s$) were generated, see Figs. 8 - 13 (d) in the appendix. These spectra are less affected by the pileup cuts, allowing the analysis from 0.6 - 6 μs, again at reduced statistics and without absolute normalization.

4 Analysis and Results

With the data ensemble shown in the appendix the $d\mu d$ kinetics was fitted separately for each temperature, according to the scheme given in Fig. 4. The calculations were done using computer code GENKIN [35].

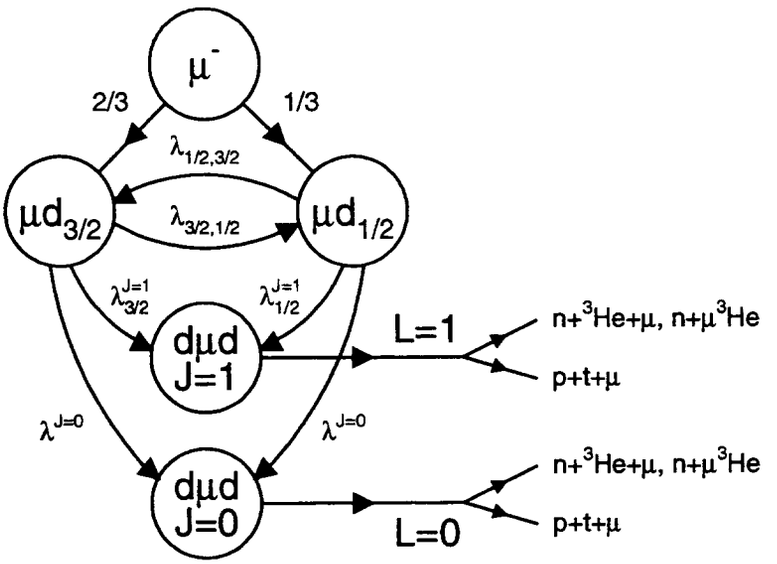

Figure 4: Kinetics scheme used for the fits of time spectra.

According to theory (see [8, 20] and references therein) the total rate of molecular formation for a given initial hfs state F, λ_F, is the sum over the final states $J = 0, 1$ of the $d\mu d$ molecule:

$$\lambda_F = \lambda^{J=0} + \lambda_F^{J=1} \tag{4}$$

Here the rate of the $(d\mu d)_{J=1}$ formation, $\lambda_F^{J=1}$, depends on the initial state F due to the contribution from the resonant mechanism. The $(d\mu d)_{J=0}$ formation is only non-resonant, and the corresponding rate $\lambda^{J=0}$ does not depend on the initial state. The formation of the $(d\mu d)_{J=1}$ state is followed by the P-wave dd fusion with the ratio of two fusion channels $(R_n/R_p)^{L=1} = 1.43$, while in the $(d\mu d)_{J=0}$ state the fusion takes place in the S-wave with $(R_n/R_p)^{L=0} = 0.886$ (the branching ratios given are from the latest R-matrix analysis of the dd fusion reactions at low energy [29]).

The rates of the spin flip transitions $F = 3/2 \leftrightarrow F = 1/2$ are connected via the detailed-balancing relation [8]:

$$\lambda_{1/2,3/2}(T) = 2e^{-\frac{\Delta}{kT}}\, \lambda_{3/2,1/2}(T) \tag{5}$$

where $\Delta = 0.0485$ eV is the hfs splitting, and T is the temperature.

Only events with a *single fusion*, i.e. not followed by any more fusions, have been selected for the present analysis. The kinetics scheme *without recycling* is thus used

in the calculations. The connection between the yields of single fusion, $Y_{n,p}^{single}$, and the yields from the first cycle, $Y_{n,p}$, is given by formulas:

$$Y_n^{single} = (1-(1-\omega_d)Y_{tot})Y_n(t) \quad (6)$$
$$Y_p^{single} = (1-Y_{tot})Y_p(t) \quad (7)$$

where Y_{tot} is the total fusion yield of the first cycle:

$$Y_{tot} = \int_0^\infty (Y_n(t) + Y_p(t))dt \quad (8)$$

In principle, five independent parameters can be determined: Two $d\mu d$ formation rates λ_F, each associated with a branching ratio of the fusion channels R_n/R_p and the spin flip rate $\lambda_{3/2,1/2}$.

The time development of the R_n/R_p ratio is plotted in Fig. 14 (appendix) for the temperatures 53 K, 73 K, 96 K and 181 K. As one can clearly recognize, there is a strong change of R_n/R_p at low temperatures, where the resonant ($F = 3/2$) $d\mu d$ formation changes with time to non-resonant ($F = 1/2$) formation. At temperatures $T \geq 100$ K resonant formation dominates for both hfs states, thus R_n/R_p remains constantly high.

Our experiment confirms, that resonant formation is associated with a P-wave branching ratio $R_n/R_p \sim 1.4$ (table 1). For the $F = 1/2$ hfs component, on the other hand, we evaluate at 53 K: $R_n/R_p \sim 1.10 \pm 0.05$, or in terms of $d\mu d_{J=0}$ formation $\lambda^{J=0} = (0.030 \pm 0.003) \cdot 10^6 s^{-1}$ which is (54±5)% of the total $\lambda_{1/2}$ rate.

The kinetic results of the fits are summarized in table 1, Fig. 6 (molecular formation rates λ_F) and Fig. 7 (spin flip rates $\lambda_{3/2,1/2}$). All results are preliminary. The first two colums of table 1 give the D_2 temperatures and muon stop numbers in the volume defined for absolute normalization. The next three colums list the $d\mu d$ formation and spin flip rates normalized to the density $\phi = 1$. Column 6 in table 1 lists the steady state formation rates $\lambda_{d\mu d}$ which were evaluated according to [8] (see also Fig. 1 for display). Columns 7 and 8 give the fusion yields per cycle Y_n and Y_p for each branch of the dd reaction, and in column 8 the evaluated ratios R_n/R_p for (mostly resonant) $d\mu d_{J=1}$ formation are given. The last column lists the χ^2 per degree of freedom of our fits. The errors given in table 1 are only statistical. For the absolute rates a systematic uncertainty of ± 2% and for the R_n/R_p ratios ~ 5% should be considered. The precision of the temperature measurements was ±3%.

The detailed results of the fits with our kinetics code are given in table 2 in the appendix and shown by the curves displayed in the Figs. 8 - 14. A comparison of the time distributions of the (n + ^{3}He) branch at the various temperatures is displayed in Fig. 5.

The sticking factor ω_d was determined from the 53 K data using the "survived muon method" [10, 23]. Our new result is $\omega_d = (12.1 \pm 0.3)\%$ in perfect agreement with the Gatchina value [11].

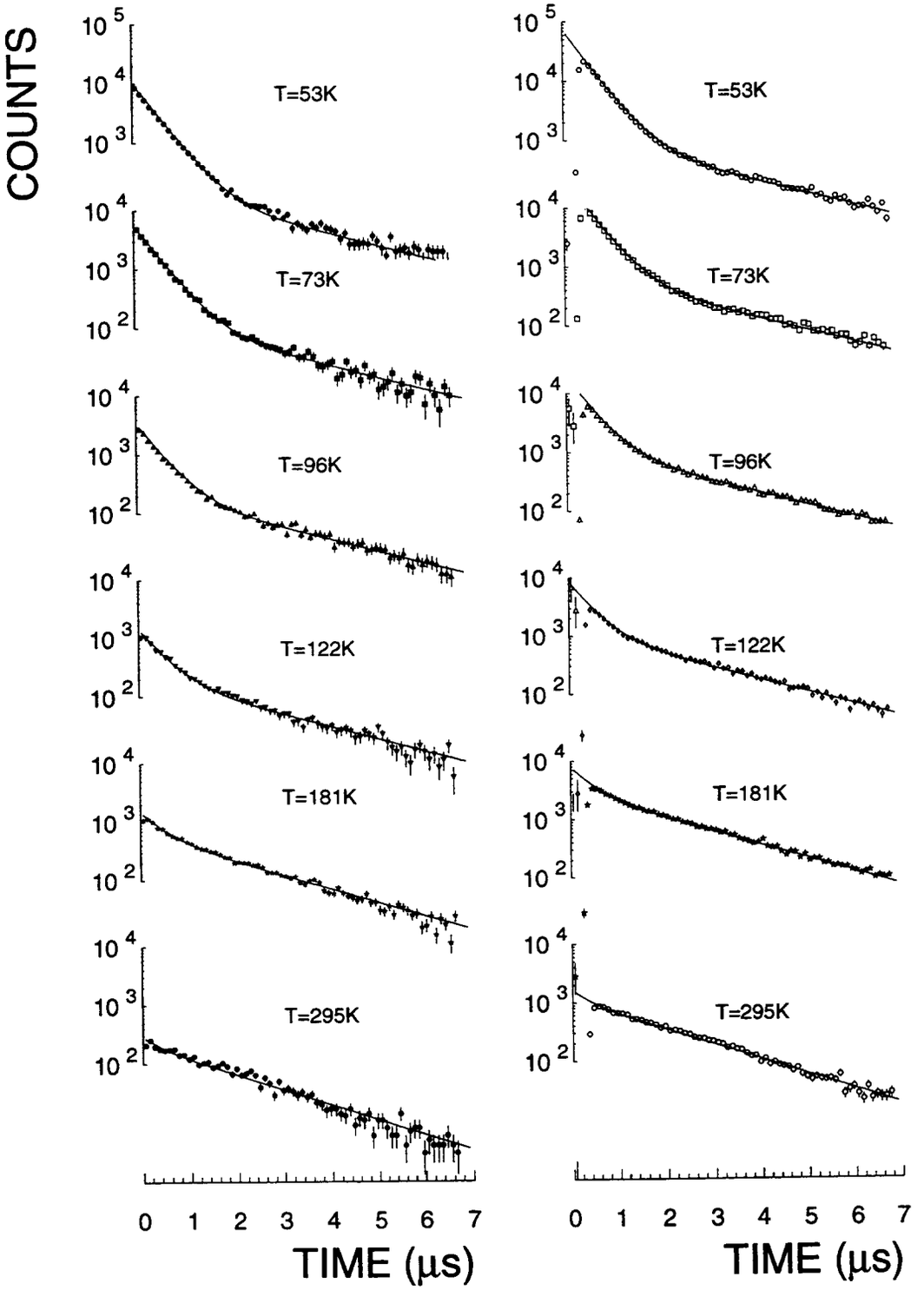

Figure 5: Comparison of time distributions of $d\mu d \rightarrow n + {}^3\mathrm{He} + \mu$ events measured at various temperatures: (left side) neutron time spectra, (right side) pure IC spectra with cut off at $t < 0.6\mu$s.

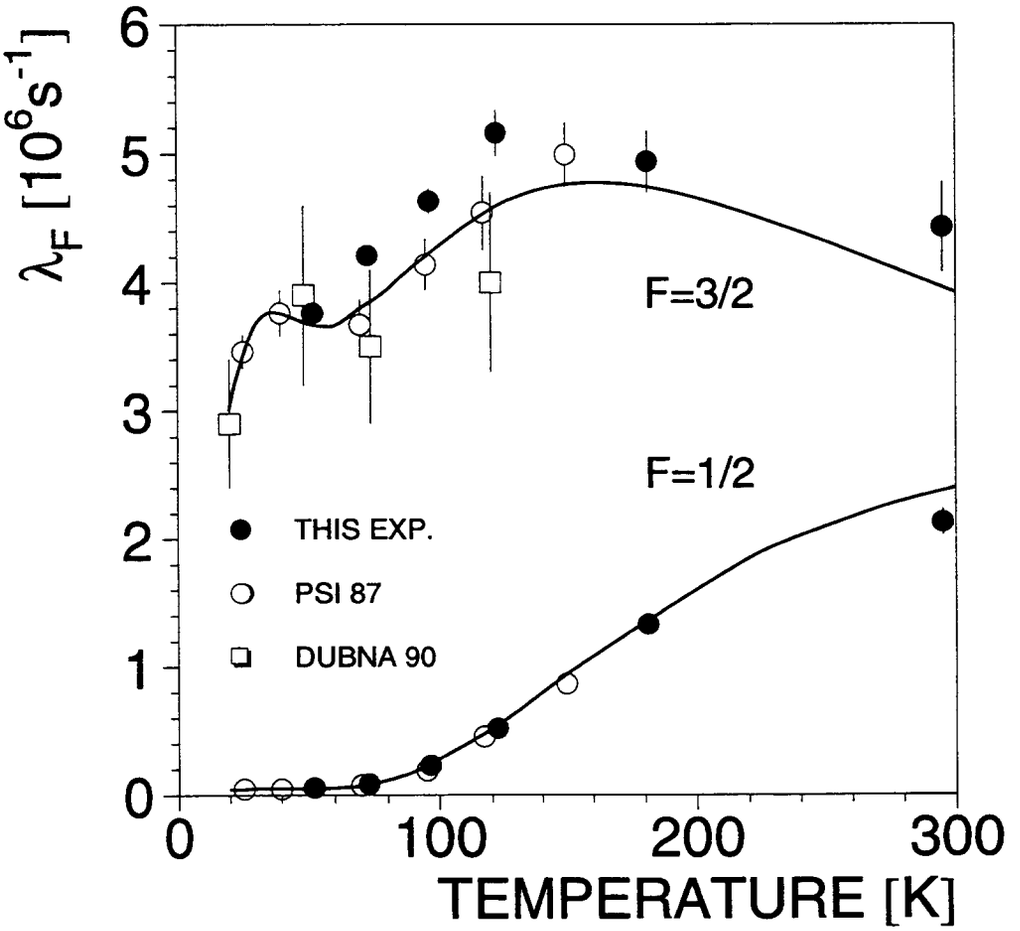

Figure 6: Kinetic fit results of the new measurements in D_2 gas at $\phi = 4.9\%$ density: Spin separated $d\mu d$ formation rates λ_F, plotted versus D_2 temperature. Also shown for comparison are all published data from previous experiments [6, 7, 14, 17] and the theory [9]. All rates are normalized to density $\phi = 1$.

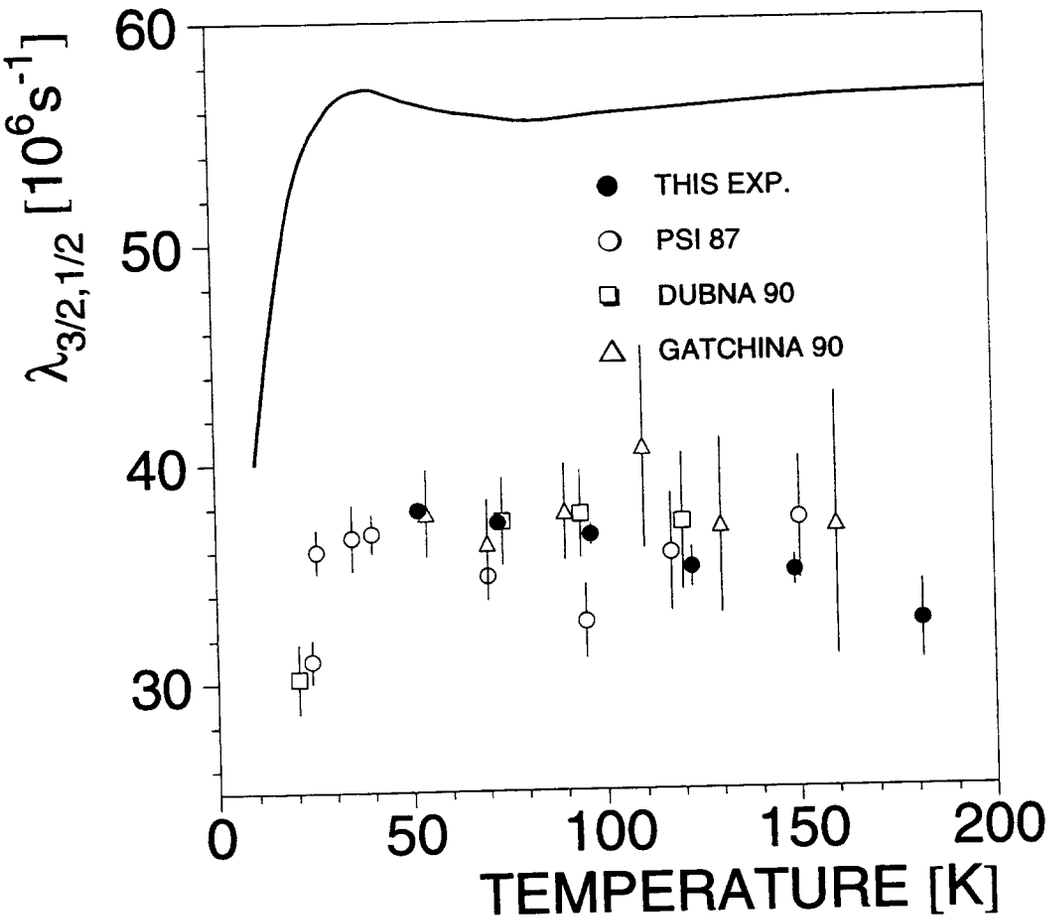

Figure 7: Plot of the evaluated spin flip rates $\lambda_{3/2,1/2}$ versus D_2 temperature and comparison with the published data from previous experiments [6, 7, 12, 14, 18] and with theoretical prediction given in [20]. All rates are normalized to density $\phi = 1$.

T K	μ 10^6	$\lambda_{1/2}$ $10^6 s^{-1}$	$\lambda_{3/2}$ $10^6 s^{-1}$	$\lambda_{3/2,1/2}$ $10^6 s^{-1}$	$\lambda_{d\mu d}$ $10^6 s^{-1}$	Y_n %	Y_p %	R_n/R_p J=1	χ^2/N
53	9.26	0.0574(5)	3.76(6)	37.84(21)	0.0612(6)	3.21	2.21	1.49(4)	1.08
73	3.79	0.0882(10)	4.21(8)	37.24(33)	0.0979(12)	3.62	2.69	1.37(4)	1.03
96	2.03	0.229(2)	4.63(10)	36.66(50)	0.271(4)	4.74	3.47	1.39(3)	1.15
122	0.814	0.520(5)	5.16(18)	35.12(92)	0.645(10)	6.50	5.19	1.26(2)	1.04
181	0.732	1.331(15)	4.94(24)	32.6(1.8)	1.69(3)	10.42	7.93	1.32(2)	1.50
295	0.152	2.13(10)	4.43(35)	(37.7)	2.68(15)	13.27	10.10	1.32(3)	1.12

Table 1: Run conditions and kinetic fit results of $d\mu d$ fusion in D_2 measured at $\phi = 4.9\%$

5 Conclusion

In this new experiment we have substantially improved the absolute accuracy of $d\mu d$ fusion data for both reaction channels ($n + {}^3$He) and ($p + t$). We agree in general with previous measurements, but find $\sim$ 5 - 10% larger formation rates λ_F than in [7]. The branching ratio R_n/R_p for the fusion from $(d\mu d)_{J=1}$ states agrees reasonably well with the P-wave branching ratio 1.43 from the R-matrix analysis [29]. For the non-resonant formation at low temperature we find that at $T = 53$ K only about 54% of the formation goes to the state $d\mu d_{J=0}$. The resonant and non-resonant formation going to the state $d\mu d_{J=1}$ cannot be separated in a *model independent* way. However it can be done using the current theory which predicts the temperature dependence of the resonant formation rate with a few fine-tuning parameters. Thus, additional precise data on the temperature dependence are needed for the further analysis. Our experiment will be continued with various D_2 and HD mixtures.

This work was supported in part by the Russian Foundation of Fundamental Research (Grant No.94-02-05082), the Austrian Science Foundation, the German Federal Ministry of Research and Technology and the Paul Scherrer Institut.

References

[1] V.P. Dzhelepov et al, Sov. Phys. JETP **19** (1964) 1376 and **23** (1966) 820.

[2] E.A. Vesman, Sov. Phys. JETP Lett. **5** (1967) 9.

[3] S.S. Gershtein and L.I. Ponomarev, Phys. Lett. **72B** (1977) 80.

[4] S.I. Vinitsky et al., Sov. Phys. JETP **47** (1978) 444.

[5] V.M. Bystritsky et al., Sov. Phys. JETP **49** (1979) 232.

[6] P. Kammel et al., Phys. Rev. Lett. **112B** (1982) 319 and Phys. Rev. **A28** (1983) 2611.

[7] J. Zmeskal et al., Muon Cat. Fusion **1** (1987) 109, and Phys. Rev. **A42** (1990) 1165.

[8] L.I. Men'shikov et al., Sov. Phys. JETP **65** (1987) 656.

[9] M.P. Faifman, Muon Cat. Fusion **2** (1988) 247 and private communication (1991).

[10] D.V. Balin et al., Phys. Lett. **141B** (1984) 173.

[11] A.A. Vorobyov, Muon Cat. Fusion **2** (1988) 17.

[12] D.V. Balin et al., Muon Cat. Fusion **5/6** (1990/91) 163.

[13] H. Bossy et al., Phys. Rev. Lett. **55** (1985) 1870 and **59** (1986) 2864.

[14] N. Nägele et al., Nuclear Physics **A493** (1989) 397.

[15] C. Petitjean et al., Muon Cat. Fusion **5/6** (1990/91) 299.

[16] S.E. Jones et al., Phys. Rev. Lett. **56** (1986) 588.

[17] V.M. Bystritsky et al., Muon Cat. Fusion **5/6** (1990/91) 141.

[18] V.V. Filchenkov and L. Marcis, Muon Cat. Fusion **5/6** (1990/91) 499.

[19] P. Kammel in *Muonic Atoms and Molecules*, eds. L. Schaller and C. Petitjean, Birkhäuser Basel 1993) p. 111.

[20] A. Scrinzi et al., Phys. Rev. **A47** (1993) 4691.

[21] C. Petitjean et al., Muon Cat. Fusion **5/6** (1990/91) 261.

[22] T. Case, Thesis (U.C. Berkeley 1993), T. Case et al., Muon Cat. Fusion **5/6** (1990/91) 327, and Hyperfine Int. **82** (1993) 295.

[23] K. Lou, Thesis (ETH Zurich, 1993), K. Lou et al., Muon Cat. Fusion **5/6** (1990/91) 525, Hyperfine Int. **82** (1993) 313, and *Muonic Atoms and Molecules*, eds. L. Schaller and C. Petitjean (Birkhäuser Basel 1993) p. 147.

[24] D.V. Balin et al., Proc. LEMS'93, (Santa Fe 1993), Los Alamos report LA-12698-C, p. 122.

[25] D.V. Balin et al., Few Body XV (Peniscola 1995), to be published (Springer-Verlag).

[26] D.V. Balin et al., Muon Cat. Fusion **5/6** (1990/91) 481.

[27] D.V. Balin et al., Muon Cat. Fusion **7** (1992) 1.

[28] L.N. Bogdanova et al., Phys. Lett. **115B** (1982) 171; **167B** (1986) 485E.

[29] G.M. Hale, Muon Cat. Fusion **5/6** (1990/91) 477.

[30] L.N. Bogdanova et al., Phys. Lett. **161B** (1985) 1.

[31] C.-Y. Hu and S.K. Kauffmann, Phys. Rev. **A36** (1987) 5420.

[32] C. Petitjean et al., Hyperfine Int. **82** (1993) 273.

[33] V.E. Markushin, Muon Cat. Fusion **3** (1988) 395.

[34] M.C. Struensee and J. Cohen, Phys. Rev. **A38** (1988) 44.

[35] E.I. Afanasieva et al., Muon Cat. Fusion **5/6** (1990/91) 477.

Appendix

T (K)	53.	73.	96.	122.	181.	295.
$N_\mu(10^6)$	9.2581	3.7932	2.0339	0.8136	0.72283	0.15198
$\lambda_{3/2}^{J=1}$	3.71(7)	4.14(12)	4.60(10)	5.13(18)	4.91(24)	4.40(35)
$\lambda_{1/2}^{J=1}$	0.0261(27)	0.0550(81)	0.199(2)	0.490(5)	1.301(15)	2.10(10)
$\lambda^{J=0}$	0.0303(26)	0.0322(80)	**0.030**			
$\lambda_{3/2,1/2}$	37.84(21)	37.26(33)	36.66(50)	35.12(92)	32.6(18)	**37.7**
$(R_n/R_p)^{J=1}$	1.52(7)	1.40(8)	1.39(3)	1.26(2)	1.32(2)	1.32(3)
χ^2/N	1.08	1.03	1.15	1.04	1.50	1.12
$Y_n(\%)$	3.21	3.62	4.74	6.50	10.42	13.27
$Y_p(\%)$	2.18	2.64	3.47	5.19	7.93	10.10
$\lambda_{3/2}$	3.73(6)	4.18(8)				
$\lambda_{1/2}$	0.0274(5)	0.0582(10)				
$\lambda^{J=0}$	**0.030**					
$\lambda_{3/2,1/2}$	37.84(21)	37.24(33)				
$(R_n/R_p)^{J=1}$	1.49(4)	1.37(4)				
χ^2/N	1.08	1.03				
$Y_n(\%)$	3.21	3.62				
$Y_p(\%)$	2.21	2.69				

Table 2: Detailed summary of results obtained by fitting *the first fusion, not followed by another one* (scheme of no recycling, but with renormalizaion of yields and muon stops, see Fig. 4). The fusion yields Y_n and Y_p are given *per cycle*. The fixed parameters are shown in bold. At $T = 53$ K and 73 K five parameters can be obtained from the fit. At higher temperature the sensitivity of the data to the $d\mu d_{J=0}$ formation is very weak, thus the rate $\lambda^{J=0}$ was fixed.

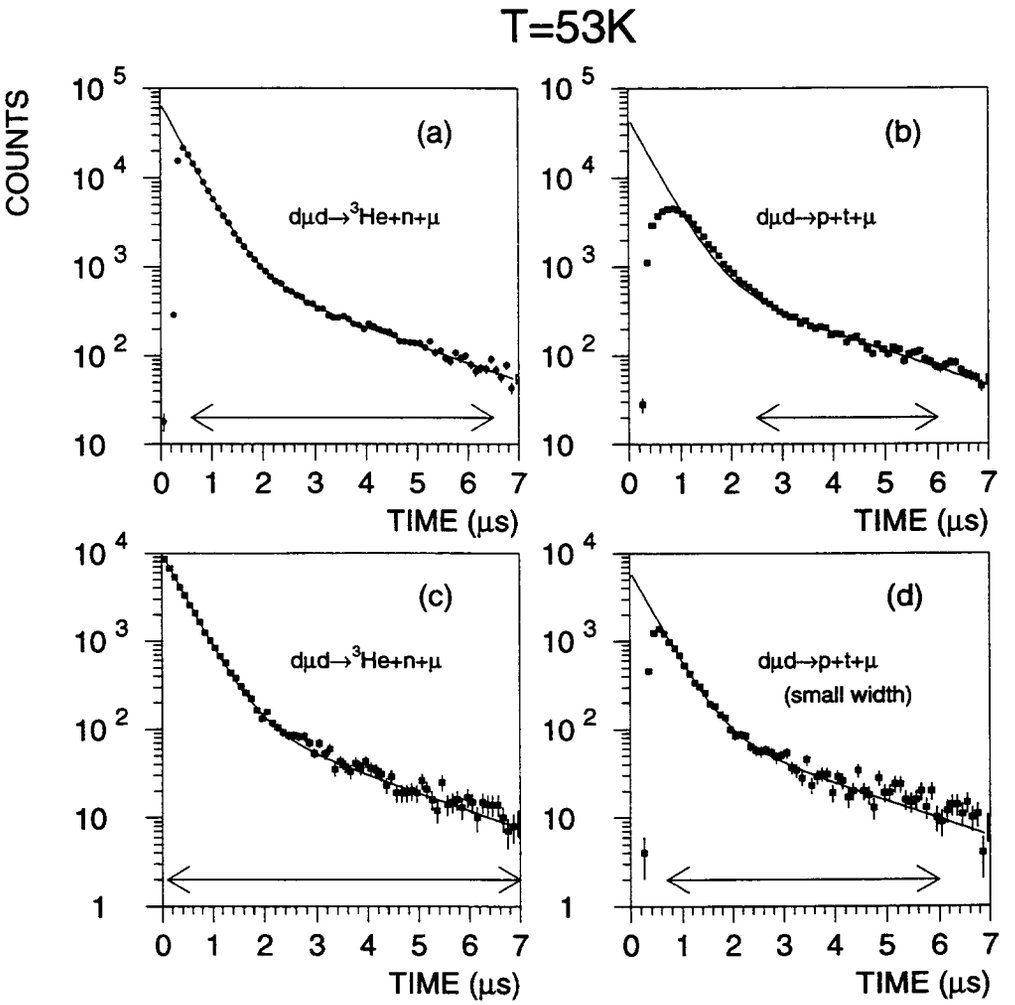

Figure 8: Time distributions measured at 53 K and fit functions: (a) IC time spectrum of μ-separated (^{3}He + μ^3He) events with absolute normalization, (b) the same for $(p + t)$ events, (c) time spectrum of neutron signals from the plastic array in coincidence with a signal μ-stop + (^{3}He/μ^3He) from the IC, (d) IC - $(p + t)$ events with small width cuts. The arrows indicate the time range used for the fits.

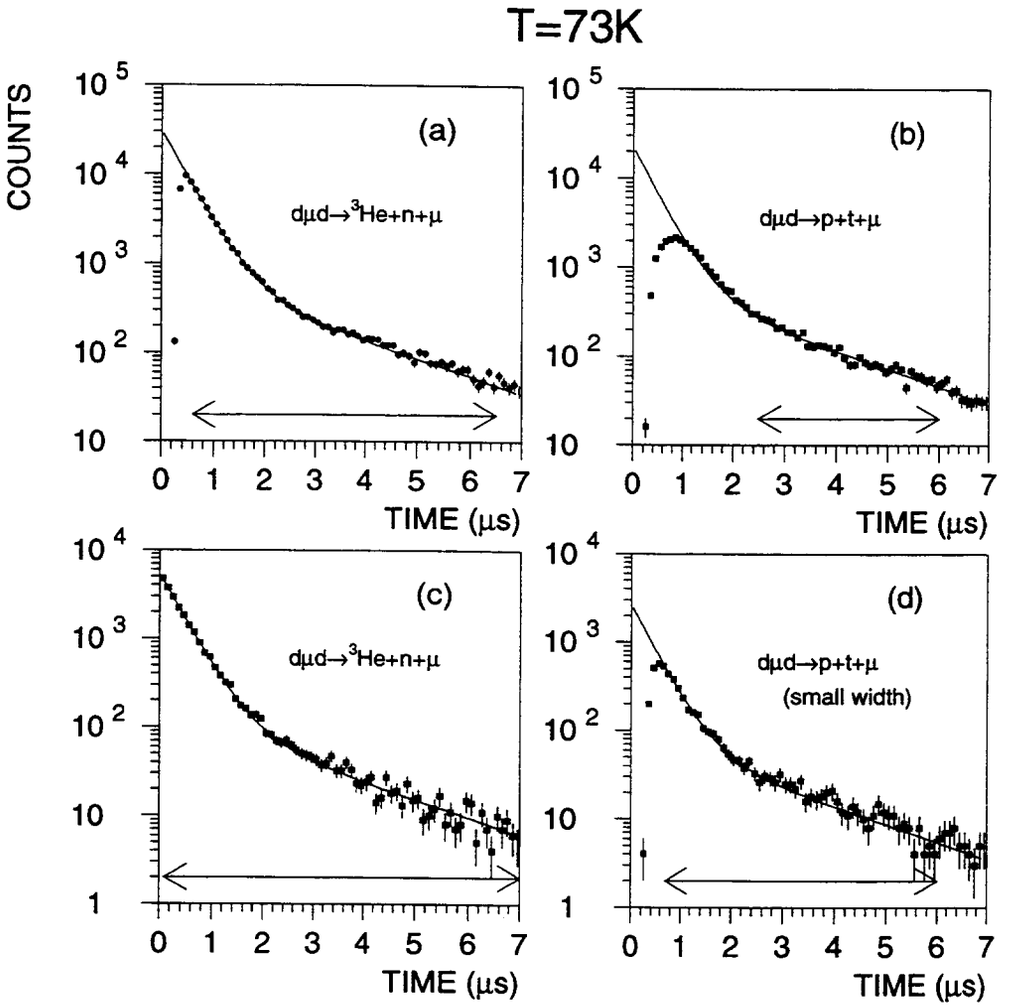

Figure 9: Time distributions measured at 73 K and fit functions: (a) IC time spectrum of μ-separated (^{3}He + μ^3He) events with absolute normalization, (b) the same for $(p + t)$ events, (c) time spectrum of neutron signals from the plastic array in coincidence with a signal μ-stop + (^{3}He/μ^3He) from the IC, (d) IC - $(p + t)$ events with small width cuts. The arrows indicate the time range used for the fits.

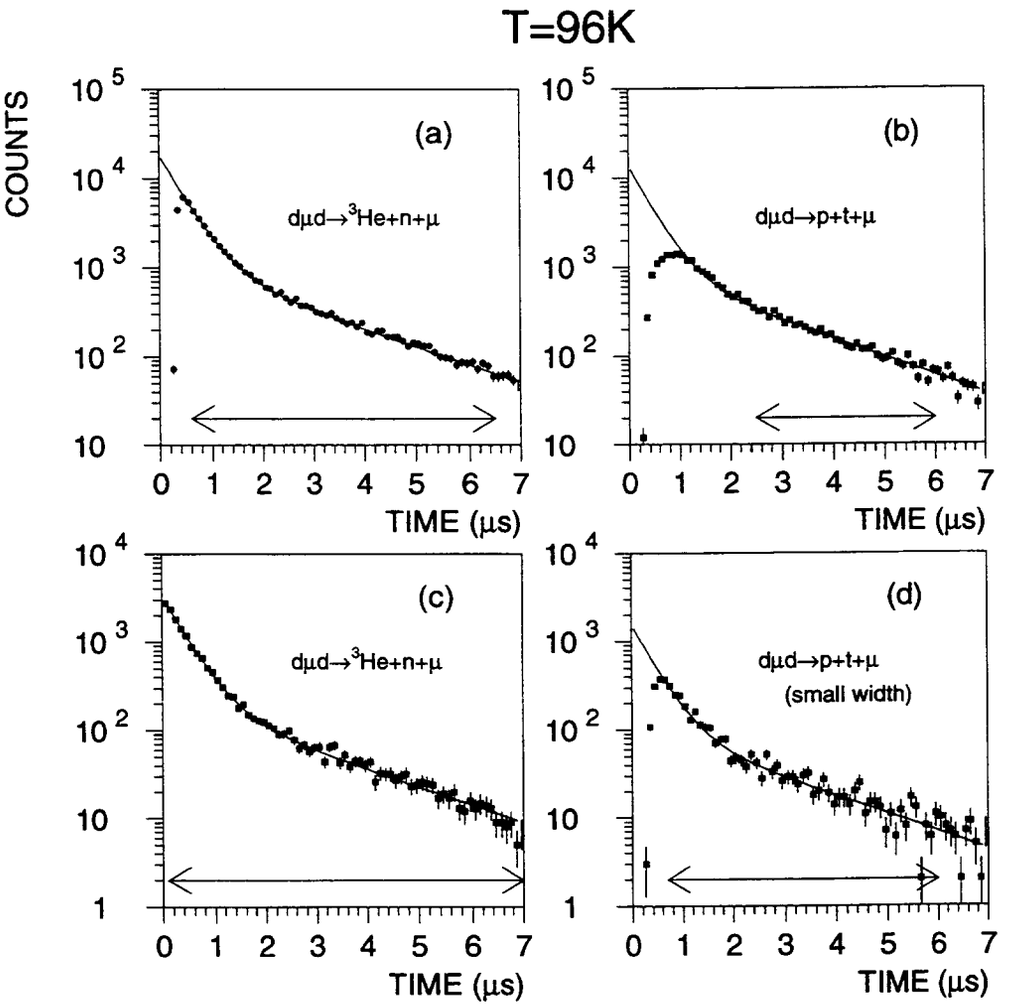

Figure 10: Time distributions measured at 96 K and fit functions: (a) IC time spectrum of μ-separated (^{3}He + μ^3He) events with absolute normalization, (b) the same for $(p+t)$ events, (c) time spectrum of neutron signals from the plastic array in coincidence with a signal μ-stop + (^{3}He/μ^3He) from the IC, (d) IC - $(p+t)$ events with small width cuts. The arrows indicate the time range used for the fits.

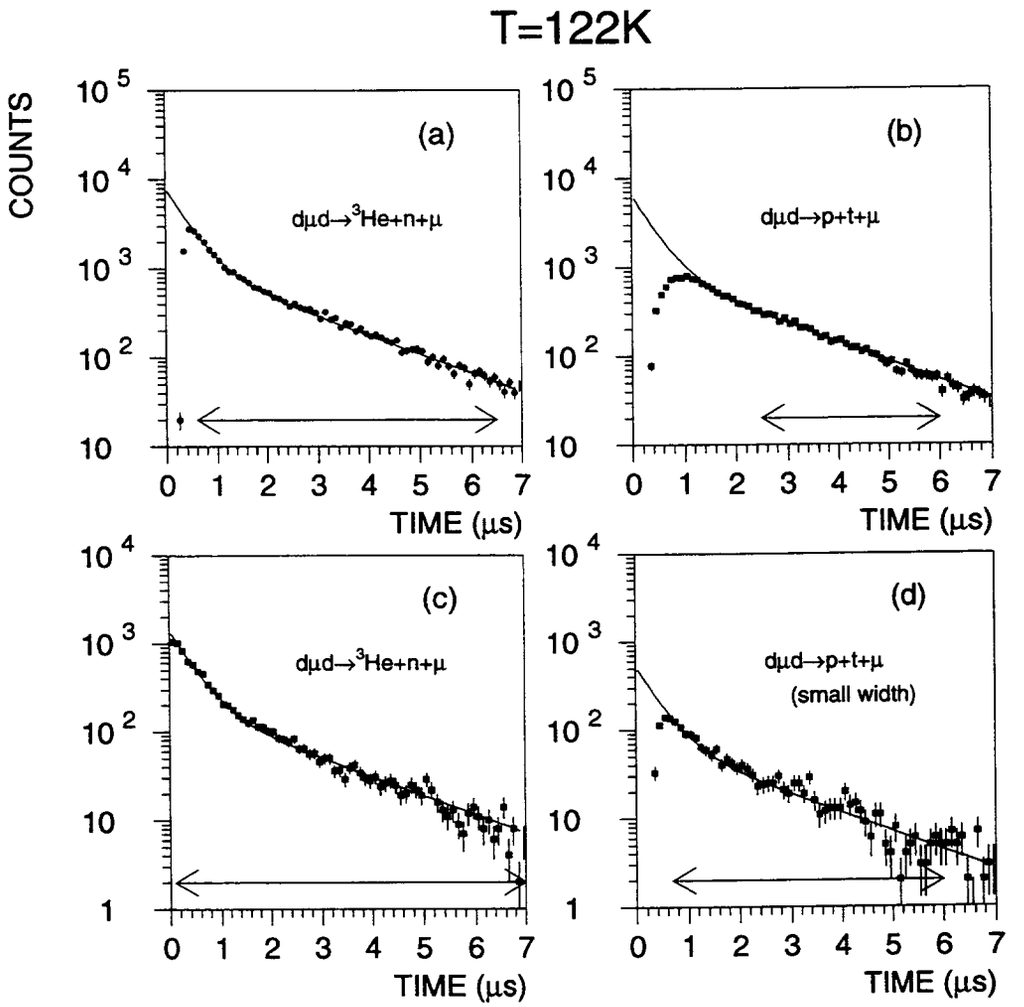

Figure 11: Time distributions measured at 122 K and fit functions: (a) IC time spectrum of μ-separated (^{3}He + μ^3He) events with absolute normalization, (b) the same for $(p+t)$ events, (c) time spectrum of neutron signals from the plastic array in coincidence with a signal μ-stop + (^{3}He/μ^3He) from the IC, (d) IC - $(p+t)$ events with small width cuts. The arrows indicate the time range used for the fits.

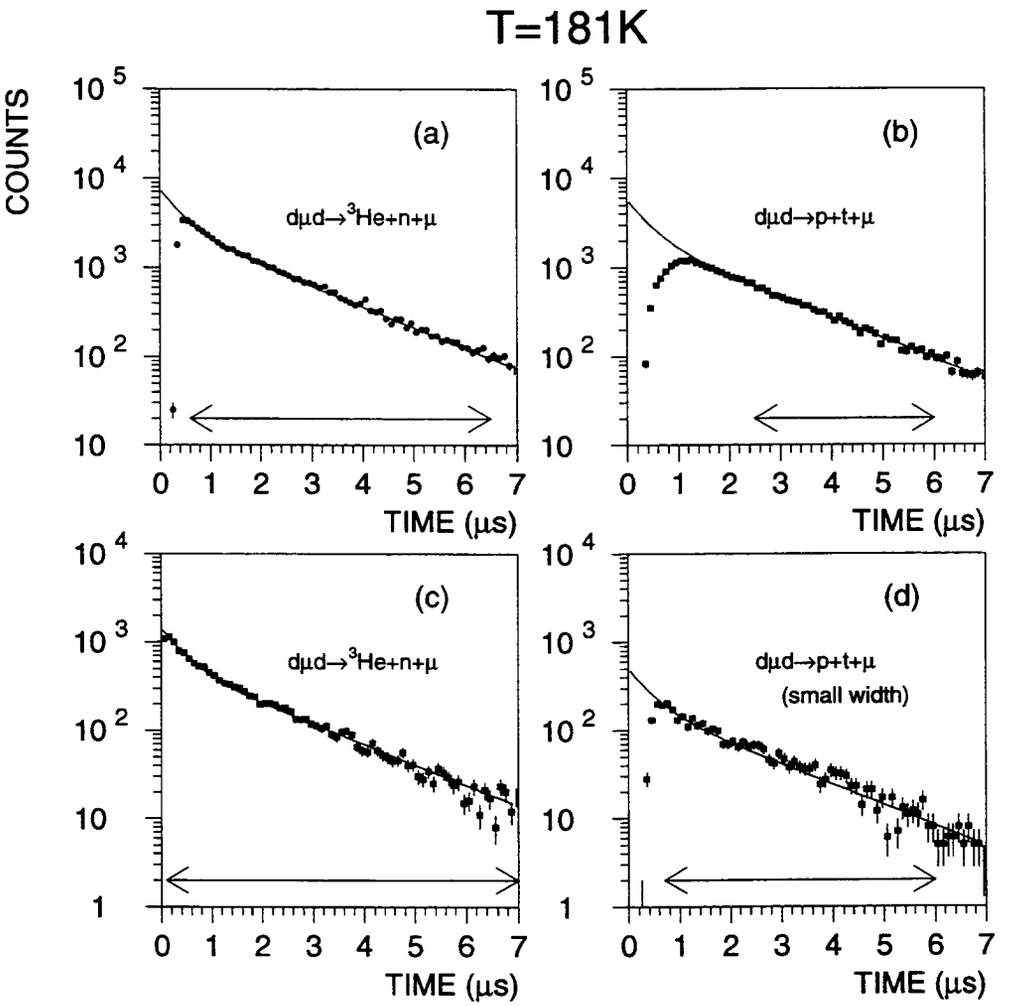

Figure 12: Time distributions measured at 181 K and fit functions: (a) IC time spectrum of μ-separated (^{3}He + μ^3He) events with absolute normalization, (b) the same for $(p+t)$ events, (c) time spectrum of neutron signals from the plastic array in coincidence with a signal μ-stop + (^{3}He/μ^3He) from the IC, (d) IC - $(p+t)$ events with small width cuts. The arrows indicate the time range used for the fits.

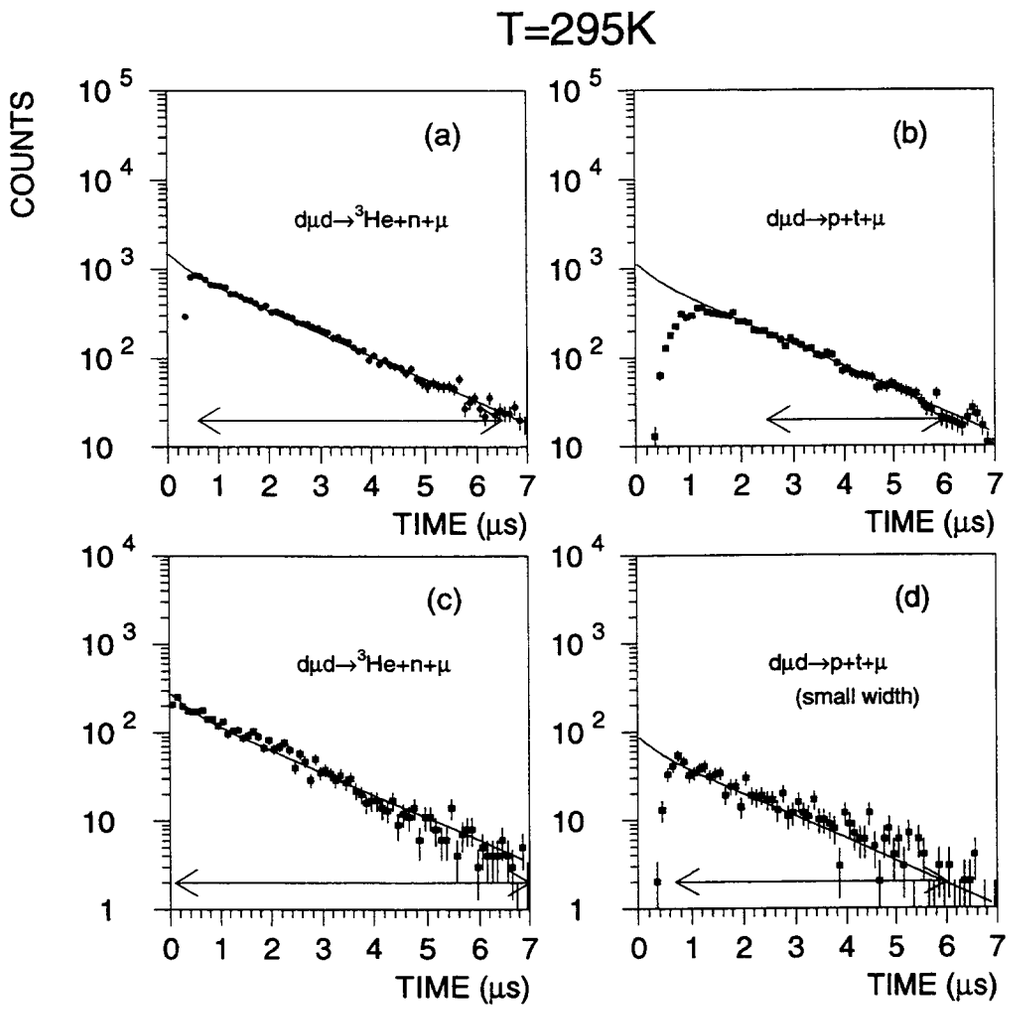

Figure 13: Time distributions measured at 295 K and fit functions: (a) IC time spectrum of μ-separated (^{3}He + μ^3He) events with absolute normalization, (b) the same for $(p+t)$ events, (c) time spectrum of neutron signals from the plastic array in coincidence with a signal μ-stop + (^{3}He/μ^3He) from the IC, (d) IC - $(p+t)$ events with small width cuts. The arrows indicate the time range used for the fits.

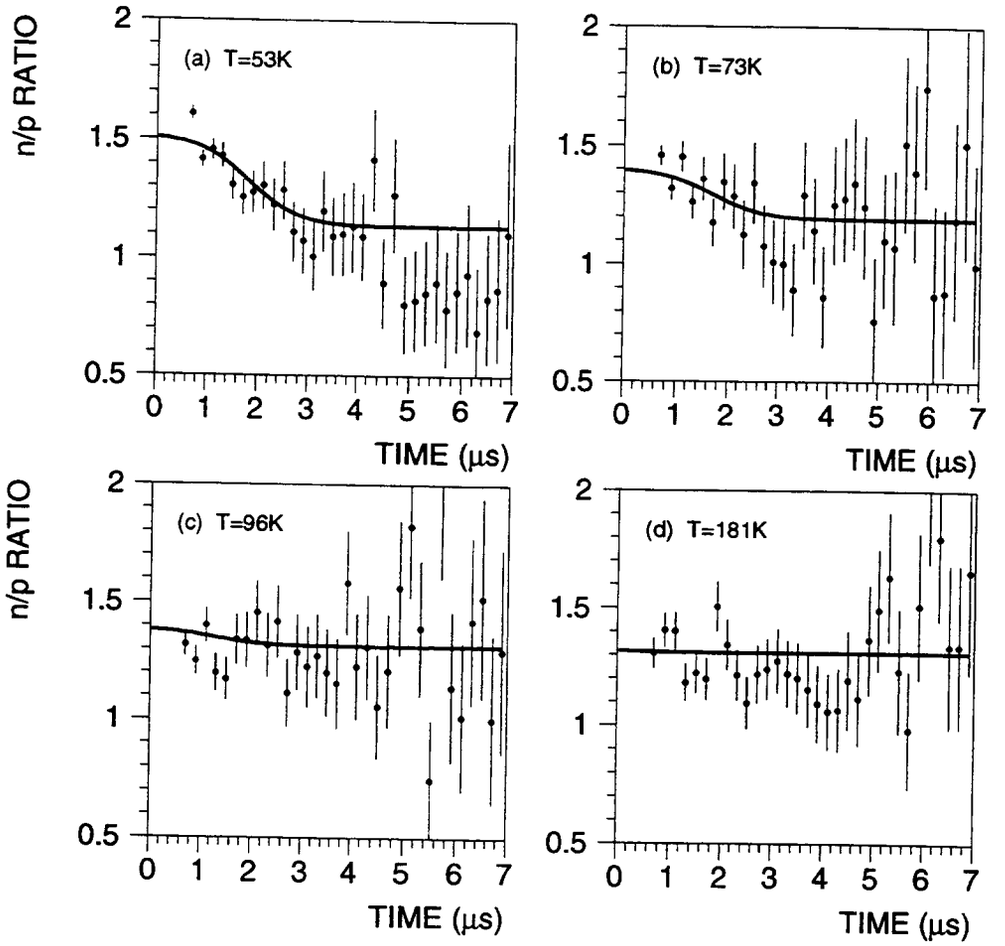

Figure 14: Time development of the ratio R_n/R_p and fit results for the temperatures (a) 53 K, (b) 73 K, (c) 96 K and (d) 181 K.